JOURNAL OF THERMOPHYSICS AND HEAT TRANSFER
Vol. 21, No. 4, October–December 2007

Effects of Buoyancy on Electrohydrodynamic-Enhanced Forced Convection in a Vertical Channel

F. C. Lai* and S. S. Kulkarni†
University of Oklahoma, Norman, Oklahoma 73019-0390

DOI: 10.2514/1.17834

Heat transfer enhancement using the electrohydrodynamic technique is numerically examined for laminar mixed convection in vertical channels. The electrical field is generated by positive corona from a wire electrode charged with a DC voltage of 15 kV. The flow Reynolds numbers considered are 600, 1200, and 1800, with Grashof numbers varying from 10^4 to 10^6 for both aiding and opposing flows. In addition to heat transfer enhancement, attention is also focused on the effect of added thermal buoyancy on the flow stability when the temperature difference between the flowing gas and bounding walls cannot be neglected.

Nomenclature

D_h = hydraulic diameter, m
d = distance between the wire and plate, m
Gr = Grashof number, $g\beta|T_i - T_w|d^3/\nu^2$
g = acceleration due to gravity, m/s^2
h = local heat transfer coefficient, W/m$^2 \cdot$ s
$\bar{h}$ = average heat transfer coefficient, W/m$^2 \cdot$ s
k = thermal conductivity of the fluid, W/m $\cdot$ s
L = length of channel, m
$\bar{L}$ = dimensionless length of the channel, L/d
Nu = local Nusselt number, hD_h/k
$\overline{Nu}$ = average Nusselt number, $\bar{h}D_h/k$
Nu_0 = average Nusselt number for forced convection without an electric field
Pe_{ehd} = Peclet number, $u_e d/\alpha$
p = pressure, Pa
Re = flow Reynolds number, $u_i d/\nu$
Re_{ehd} = electrohydrodynamic Reynolds number, $u_e d/\nu$
T = temperature, K
T_i = inlet air temperature, K
T_m = mean air temperature at a given cross section of the channel, K
T_w = wall temperature, K
t = time, s
u = velocity in the x direction, m/s
u_e = characteristic velocity of the ionic wind, $\sqrt{\rho_{\text{co}} V_o/\rho}$, m/s
u_i = uniform velocity at the inlet, m/s
$\bar{u}_i$ = dimensionless inlet velocity of air, u_i/u_e
V = electric potential, V
$\bar{V}$ = normalized electrical potential, V/V_o
V_o = electric potential at the wire, V
v = velocity in the y direction, m/s
X, Y = dimensionless Cartesian coordinates, x/d, y/d
x, y = Cartesian coordinates, m
α = thermal diffusivity, m^2/s
β = coefficient of thermal expansion, 1/K
ε_0 = permittivity of free space, F/m
θ = dimensionless temperature, $(T - T_w)/(T_i - T_w)$
θ_o = dimensionless mean outlet air temperature
ν = kinematic viscosity of the fluid, m^2/s
ρ = fluid density, kg/m^3
ρ_c = charge density, C/m^3
$\bar{\rho}_c$ = dimensionless charge density, ρ_c/ρ_{co}
ρ_{co} = charge density at the wire, C/m^3
τ = dimensionless time, $u_e t/d$
Ψ = dimensionless stream function, $\psi/u_e d$
ψ = stream function, m^2/s
Ω = dimensionless velocity, $\omega d/u_e$
ω = vorticity, 1/s

Received 23 May 2005; revision received 9 April 2007; accepted for publication 10 April 2007.

*Associate Professor, School of Aerospace and Mechanical Engineering; flai@ou.edu. Associate Fellow AIAA (Corresponding Author).

†Graduate Research Assistant, School of Aerospace and Mechanical Engineering.

Introduction

ENHANCEMENT of heat transfer has been a subject of major interest for many decades. Among the available techniques, one that employs electrohydrodynamics (EHD) seems to be the most attractive because of its simplicity and low power requirement. The mechanism for EHD heat enhancement arises from the electric body force. For single-phase flows, the coupling between a high-voltage electric field with a flowfield gives rise to an electrically induced secondary flow, which is also known as corona wind. This EHD-induced secondary flow can be thought of as a microjet of fluid issuing from the charged electrode to the grounded heat transfer surface. The net effect of this secondary flow is additional mixing of flow and destabilization of the thermal boundary layer, thus leading to a substantial increase in heat transfer coefficients. Despite the fact that EHD operation is now generally understood and its use in heat transfer enhancement has been successfully demonstrated, many questions regarding the enhancement mechanisms still remain unanswered.

Previous studies have primarily emphasized the role of the electric body force in the creation of secondary flows. Very limited results have been reported on the interaction between the flow and electrostatic fields. The interaction of the electric wind with a superimposed external flow was first investigated by Yamamoto and Velkoff [1]. The study was reexamined later by Lai et al. [2] to reveal the existence of steady-periodic flows. Although the existence of EHD-induced oscillatory flows was also noticed by Takimoto et al. [3] in their experimental study of EHD flows, the relation among the oscillatory frequency, Reynolds number, and dimensionless EHD number was not fully disclosed until recently [2]. From the heat transfer point of view, it is speculated that the oscillatory flows thus generated may lead to an additional increase in the heat transfer between the flowing gas and the bounding walls. Subsequent studies conducted by one of the authors have indeed confirmed this speculation [4,5]. In addition, the results have shown that thermal buoyancy may have a compound influence on the flow stability, because transitions from steady-periodic flow to nonperiodic flow

have been observed when the buoyancy strength (i.e., the Grashof number) becomes large [4].

For flows in a vertical channel, the thermal buoyancy along with the electrical body forces may play an important role in the creation of secondary flows. This in turn may affect the heat transfer through the channel walls in the presence of oscillatory flow. It is the purpose of this study to investigate the heat transfer enhancement for flows in a vertical channel under the influence of an electric field. Attention is also focused on the effect of thermal buoyancy on the stability of flow and temperature fields.

Formulation and Numerical Method

The geometry considered is a two-dimensional vertical channel in which a wire electrode charged with a DC high voltage is placed in the center of the channel, whereas the two bounding walls, maintained at a constant temperature T_w, are electrically grounded (Fig. 1). Because the positive corona discharge is uniform along the length of the wire, it permits a two-dimensional analysis [1–3], whereas a negative discharge would not simplify to two dimensions. As such, only positive corona discharge is considered in the present study. Uniform airflow at a constant velocity u_i and temperature T_i ($T_i < T_w$) is introduced at the channel inlet. The flow is designated as an "aiding flow" when thermal buoyancy is in the same direction as that of the primary flow and, likewise, as an "opposing flow" when it is in the opposite direction to that of the primary flow. Both aiding and opposing flows are considered in the present study. The length of the channel is set to be seven times the distance between the wire and plate (i.e., $L/d = 7$). This geometry, which is identical to that used by Yamamoto and Velkoff [1], is chosen so that the previously reported electric field data can be used for the present numerical calculations.

The governing equations of the electrical field are given by [2,4,5]

$$\frac{\partial^2 V}{\partial x^2} + \frac{\partial^2 V}{\partial y^2} = -\frac{\rho_c}{\varepsilon_0} \tag{1}$$

$$\rho_c^2 = \varepsilon_0 \left(\frac{\partial \rho_c}{\partial x}\frac{\partial V}{\partial y} + \frac{\partial \rho_c}{\partial y}\frac{\partial V}{\partial x} \right) \tag{2}$$

which can be readily derived from Maxwell's equations and Ohm's law. In the derivation of the preceding equations, it was assumed that the ion drift velocity (on the order of 10 m/s, depending on the electric field strength) is much greater than the air velocity (varying from 0.15 to 0.45 m/s for the present study), such that the contribution of convective flow to the current density can be neglected. Also, the electrodynamic and fluid dynamic equations can be decoupled for the same reason. Thus, the electric field can be solved independently of the flow and temperature fields. Although accepted as a common practice, this so-called one-way coupling approach has been verified only recently [6]. No convergence problems were encountered with this solution method. The corresponding boundary conditions are given as follows:

At the wire:

$$V = V_o \tag{3a}$$

Along the channel wall ($y = d$):

$$V = 0 \tag{3b}$$

Along the centerline ($y = 0$):

$$\frac{\partial V}{\partial y} = 0 \tag{3c}$$

The governing equations for the flow and temperature fields are given by [4]

$$\frac{\partial u}{\partial x} + \frac{\partial v}{\partial y} = 0 \tag{4}$$

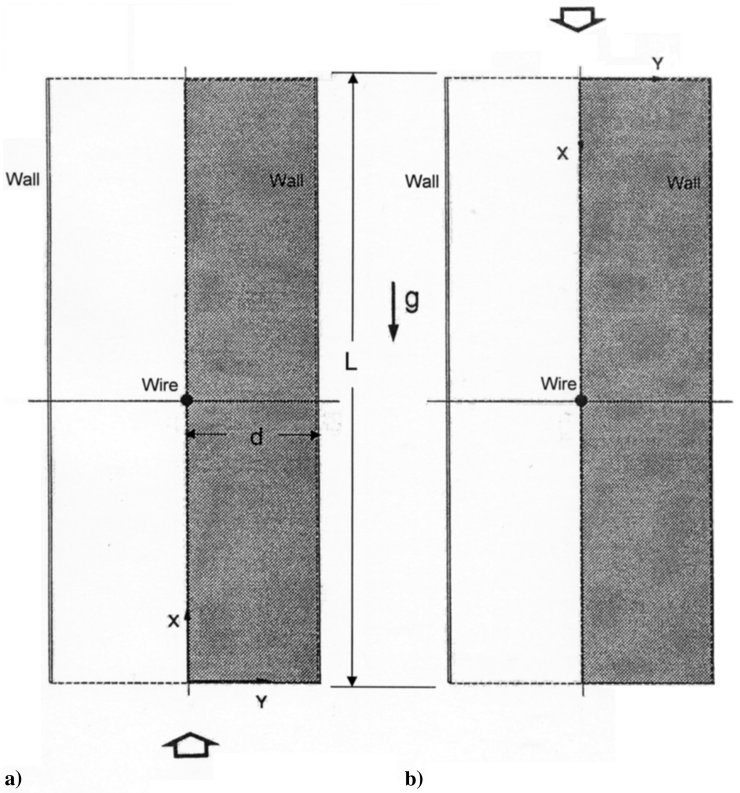

Fig. 1 Vertical channel with an electrode wire ($d = 3$ cm and $L = 21$ cm): a) aiding flow and b) opposing flow.

$$\frac{\partial u}{\partial t}+u\frac{\partial u}{\partial x}+v\frac{\partial u}{\partial y}=-\frac{1}{\rho}\frac{\partial p}{\partial x}+\nu\left(\frac{\partial^2 u}{\partial x^2}+\frac{\partial^2 u}{\partial y^2}\right)-\frac{\rho_c}{\rho}\frac{\partial V}{\partial x}\pm g\beta(T-T_w) \tag{5}$$

$$\frac{\partial v}{\partial t}+u\frac{\partial v}{\partial x}+v\frac{\partial v}{\partial y}=-\frac{1}{\rho}\frac{\partial p}{\partial y}+\nu\left(\frac{\partial^2 v}{\partial x^2}+\frac{\partial^2 v}{\partial y^2}\right)-\frac{\rho_c}{\rho}\frac{\partial V}{\partial y} \tag{6}$$

$$\frac{\partial T}{\partial t}+u\frac{\partial T}{\partial x}+v\frac{\partial T}{\partial y}=\alpha\left(\frac{\partial^2 T}{\partial x^2}+\frac{\partial^2 T}{\partial y^2}\right) \tag{7}$$

The third term on the right-hand side of Eqs. (5) and (6) represents the body force term due to the electrical field. The plus sign in front of the thermal buoyancy term, the last term in Eq. (5), represents opposing flows, whereas the minus sign is for adding flows. For the geometry considered, the electric current involved is very small (on the order of 10^{-5} A, based on the measurements of Yamamoto [7]) over the range of voltage applied, which justified the neglect of Joule heating.

The preceding equations can be nondimensionalized and expressed in terms of stream function and vorticity, which eliminates the need for calculating the pressure distribution in the solution of the flowfield and thus greatly simplifies the numerical calculations:

$$\frac{\partial^2\Psi}{\partial X^2}+\frac{\partial^2\Psi}{\partial Y^2}=-\Omega \tag{8}$$

$$\frac{\partial\Omega}{\partial\tau}=\frac{\partial\Psi}{\partial}\frac{\partial\Omega}{\partial Y}-\frac{\partial\Psi}{\partial Y}\frac{\partial\Omega}{\partial X}+\frac{1}{Re_{\text{ehd}}}\left(\frac{\partial^2\Omega}{\partial X^2}+\frac{\partial^2\Omega}{\partial Y^2}\right)+\left(\frac{\partial\bar{\rho}_c}{\partial X}\frac{\partial\bar{V}}{\partial Y}-\frac{\partial\bar{\rho}_c}{\partial Y}\frac{\partial\bar{V}}{\partial X}\right)\pm\frac{Gr}{Re_{\text{ehd}}^2}\frac{\partial\theta}{\partial Y} \tag{9}$$

$$\frac{\partial\theta}{\partial\tau}=\frac{\partial\Psi}{\partial X}\frac{\partial\theta}{\partial Y}-\frac{\partial\Psi}{\partial Y}\frac{\partial\theta}{\partial X}+\frac{1}{Pe_{\text{ehd}}}\left(\frac{\partial^2\theta}{\partial X^2}+\frac{\partial^2\theta}{\partial Y^2}\right) \tag{10}$$

The corresponding boundary conditions for the flow and temperature fields are given by

$$X=0,\qquad \Omega=0,\qquad \Psi=\bar{u}_i Y,\qquad \theta=1 \tag{11a}$$

$$X=\bar{L},\qquad \frac{\partial\Omega}{\partial X}=0,\qquad \frac{\partial\Psi}{\partial X}=0,\qquad \frac{\partial\theta}{\partial X}=0 \tag{11b}$$

$$Y=0,\qquad \Omega=0,\qquad \Psi=0,\qquad \frac{\partial\theta}{\partial Y}=0 \tag{11c}$$

$$Y=1,\qquad \Omega=\frac{\partial^2\Psi}{\partial Y^2},\qquad \Psi=\bar{u}_i,\qquad \theta=0 \tag{11d}$$

At the channel exit [Eq. (11d)], gradients of stream function, vorticity, and temperature are set to zero. These boundary conditions are less restrictive and are widely accepted [8,9].

For the present study, the electric field is created by a wire placed at the center of the channel, which carries a DC voltage of 15 kV. A positive corona discharge is considered because it is inherently more stable and uniform than a negative corona [10,11]. Because of symmetry, only one-half of the channel is required for the numerical calculations. The computational domain is shown as a shaded area in Fig. 1. For the solution of the electric field, the numerical procedure employed to solve Eqs. (1) and (2) is identical to that used by Yamamoto and Velkoff [1]. Electric potential and charge density are determined by iteration of Eqs. (1) and (2), with an assumed value of space charge density at the wire (ρ_{co}). The validity of the solution is checked by comparing the total predicted current to measured current at a specific operating voltage (for the present study, the total current involved is 4×10^{-5} A, as reported by Yamamoto [7]). If the currents do not match, a new value of space charge density at the wire is assumed and the calculations are repeated. When the electric field solutions converge, the charge density at the wire is found to be 8.66×10^{-4} C/m^3. The solutions of the flow and temperature fields are obtained using the standard procedure for the stream function–vorticity formulation, which is well documented in most numerical textbooks (e.g., Jaluria and Torrance [8] and Roache [9]) and is thus omitted, for brevity.

To evaluate the heat transfer performance, one needs to calculate the heat transfer coefficient. The local heat transfer coefficient in terms of the local Nusselt number is given by

$$Nu=\frac{hD_h}{k}=\frac{qD_h}{k(T_w-T_m)}=\frac{D_h(\partial T/\partial y)}{T_w-T_m} \tag{12}$$

In the preceding expression, D_h is the hydraulic diameter and T_m is the fluid bulk temperature at the given cross section. Similarly, the average heat transfer coefficient can be determined from the average Nusselt number, which is given by

$$\overline{Nu}=\frac{4}{\bar{L}}\frac{\log(1/\theta_0)}{1-\theta_0}\int_0^{\bar{L}}\left.\frac{\partial\theta}{\partial Y}\right|_{Y=1}\mathrm{d}X \tag{13}$$

Numerical solution starts with the calculations of electric field, then is followed by solving the flow and temperature fields simultaneously. A uniform grid (225×33) is chosen for the present study, which is the same as the previous study [2] for the same channel configuration. Because the test of grid dependence has been conducted by one of the authors in the previous study [2], there is no need for repetition. Also, because the radius of the electrode wire (10^{-4} m) is rather small compared with the grid spacing used (9.375×10^{-4} m), it is appropriate to treat the wire as a nodal point. The dimensionless time step chosen is 5×10^{-4}, to guarantee numerical stability and accuracy. The stability criterion for the numerical scheme used is given by Jaluria and Torrance [8]:

$$\Delta t\le\frac{1}{2\nu\left[\frac{1}{(\Delta x)^2}+\frac{1}{(\Delta y)^2}\right]+\frac{|u|}{\Delta x}+\frac{|v|}{\Delta y}} \tag{14}$$

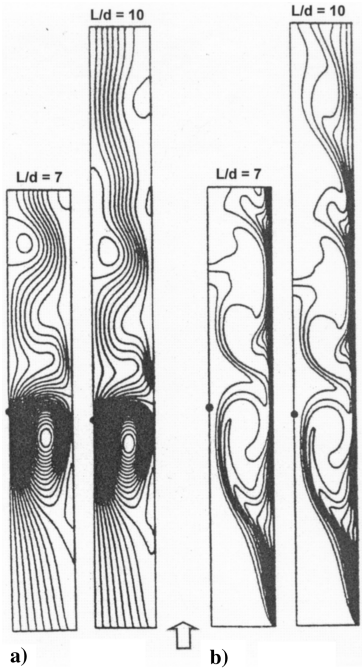

Fig. 2 Effect of channel length on the numerical results ($V_o=15$ kV, $Gr=0$, and $Re=600$): a) flowfield ($\Delta\psi=0.006$) and b) temperature field ($\Delta\theta=0.1$).

To ensure that the channel length used is adequate to reveal the physical phenomena involved, calculations were performed on an extended domain ($L/d = 10$). Only slight differences in the streamline and isotherm patterns are found near the channel exit. The flow and temperature fields are otherwise the same (Fig. 2). These subtle differences do not modify the flow periodicity and produce only less than 0.2% difference in the Nusselt number. Also, to verify that the observed oscillations are not due to numerical instability, computations were repeated with a reduced time step ($\Delta\tau = 1\times 10^{-4}$). The results thus obtained are nearly identical to those using the time step of $\Delta\tau = 5 \times 10^{-4}$ in the prediction of flow periodicity and calculated Nusselt numbers. Calculations have covered a wide range of parameters ($10^4 \leq Gr \leq 10^6$ and $Re = 600$, 1200, and 1800), with particular attention being placed on the stability of the flow and temperature fields due to the added thermal buoyancy. To closely monitor the development of the flow and temperature fields, the computation is continued until a steady state or steady-periodic state is reached.

Results and Discussion

For forced convection in the absence of an electrical field, it was observed that the flow and temperature fields all reach steady state, with Fig. 3 showing the final steady-state results achieved. The thermal boundary layer becomes thinner with an increase in the Reynolds number, thus leading to an increase in heat transfer. The results obtained for the average Nusselt number in general agree well with the correlation reported by Shah and London [12]. The small differences observed (which vary from 1 to 6%, depending on the Reynolds number) in the Nusselt numbers obtained in this analysis and those tabulated by Shah and London may be attributed to neglecting axial diffusion in the latter analysis.

For forced convection in the presence of an electrical field, the flow and temperature fields are shown in Fig. 4. With the application of an electrical field, the flow and temperature fields become oscillatory at $Re = 600$ and 1200. Only one recirculating cell is observed for flows at $Re = 1200$ and 1800, whereas multiple cells are observed for flow at $Re = 600$. As reported by Lai et al. [2], there is a strong connection between the stability of the flow and its flow structure (i.e., single cell or multiple cells). The thermal boundary layer is perturbed by the electric field near the wire when it extends over the recirculating flow region. The thermal boundary layer is stabilized past the wire when steady state is reached, a phenomenon similar to that prevailing in forced convection without an electrical field. The oscillatory temperature field in the presence of an electric field is distinguished by a wavelike appearance of the thermal boundary layer downstream.

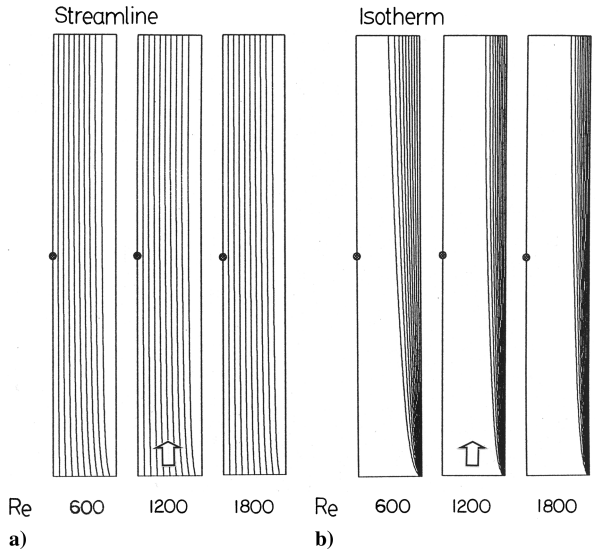

Fig. 3 Forced convection in a channel without electric field, $Gr = 0$: a) flowfield ($\Delta\psi = 0.006$ for $Re = 600$, $\Delta\psi = 0.009$ for $Re = 1200$, and $\Delta\psi = 0.014$ for $Re = 1800$) and b) temperature field ($\Delta\theta = 0.1$).

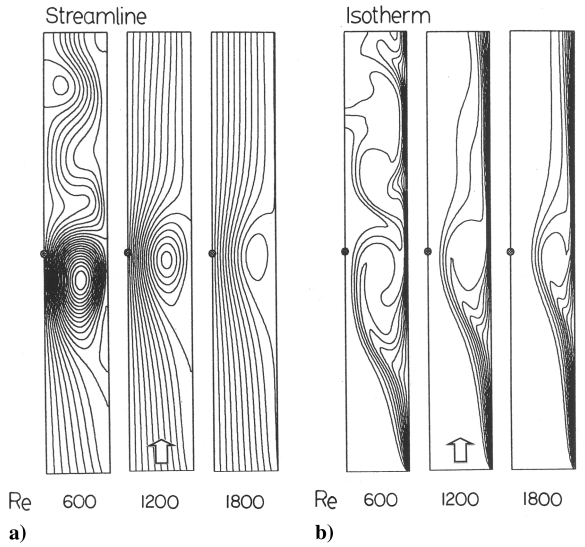

Fig. 4 Forced convection in a channel with electric field, $Gr = 0$: a) flowfield (flows at Re $= 600$ and 1200 are oscillatory; $\Delta\psi = 0.006$ for $Re = 600$, $\Delta\psi = 0.009$ for $Re = 1200$, and $\Delta\psi = 0.014$ for $Re = 1800$) and b) temperature field ($\Delta\theta = 0.1$).

To assess the heat transfer enhancement in forced convection, the Nusselt number obtained in the presence of the electric field is compared with that without the electric field. Through our overall experience in this study, it is found that an increase in the flow inertia (i.e., the Reynolds number) results in declining heat transfer enhancement, which is consistent with the results reported in [5]. For example, the increase in heat transfer is 168% for $Re = 600$ and 135% for $Re = 1800$. The reason for this reduction in heat transfer enhancement is due to the suppression of the EHD-induced secondary flow. The trend observed here is also consistent with the experimental results reported by Takimoto et al. [3]

When thermal buoyancy is involved, the flow and temperature fields become even more complicated. To investigate the effect of thermal buoyancy on the stability of flow and temperature fields, the flow and electric field conditions are fixed (i.e., u_i and V_o are maintained at a constant value) whereas the buoyancy strength, represented by the Grashof number, is increased.

At $Re = 1800$, the flow and temperature fields remain stable as the Grashof number is increased from 10^4 to 10^6. The flow and temperature fields do not show any oscillation and they all reach steady state. Figures 5 and 6 show the resulting steady-state flow and

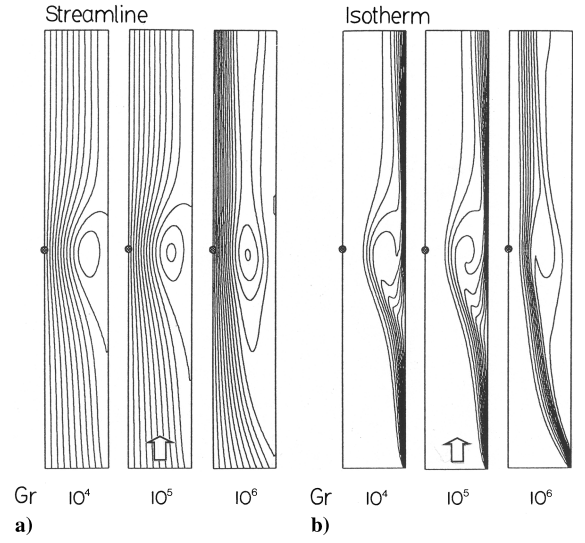

Fig. 5 Mixed convection for aiding flows at $Re = 1800$: a) flowfield ($\Delta\psi = 0.014$) and b) temperature field ($\Delta\theta = 0.1$).

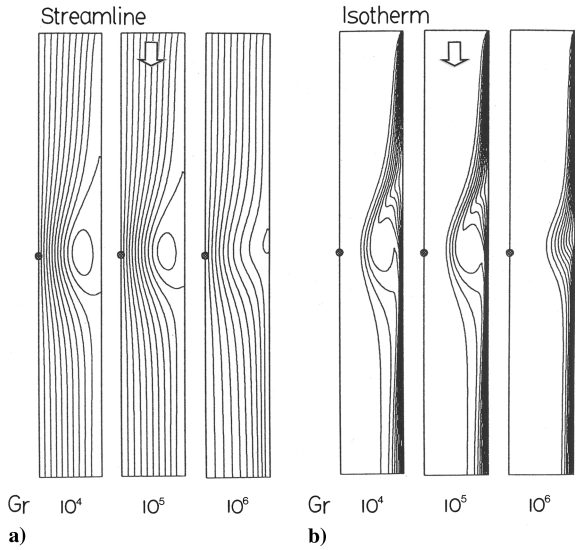

Fig. 6 Mixed convection for opposing flows at $Re = 1800$: a) flowfield ($\Delta\psi = 0.014$) and b) temperature field ($\Delta\theta = 0.1$).

temperature fields for aiding and opposing flows, respectively. When thermal buoyancy is weak (i.e., $Gr = 10^4$), it is observed that the flow patterns for both aiding and opposing flows are similar to that of forced convection (Fig. 4). With an increase in the buoyancy strength, it is observed that the strength of the recirculating cell increases for aiding flows (Fig. 5). As a result, flow reversal occurs at the exit of the channel in which the ambient air is brought into the channel when the Grashof number is increased to 10^6. Because of this entrainment of colder air from the ambient, the primary flow (i.e., the warmer air) is confined to the central region of the channel, which has a significant effect on the heat transfer, as will be elaborated later in the discussion of the heat transfer results. For opposing flows, on the other hand, the strength of secondary flow is reduced as the Grashof number increases, which leads to a thinner thermal boundary layer (Fig. 6).

At $Re = 1200$, both aiding and opposing flows become periodic when $Gr = 10^4$. Because thermal buoyancy is weak in this case, the periodicity of oscillation for both aiding and opposing flows is almost identical to that of forced convection (Fig. 4). As the Grashof number is increased to 10^5, the opposing flow stabilizes, whereas the aiding flow remains oscillatory. For the latter case, the variations of flow and temperature fields with time are shown in Figs. 7 and 8, respectively, for approximately a complete cycle ($\approx$34 units of dimensionless time). From these figures, one can clearly observe the variation of the secondary flow strength with time and its effect on the wavelike thermal boundary layer downstream of the wire. This interesting

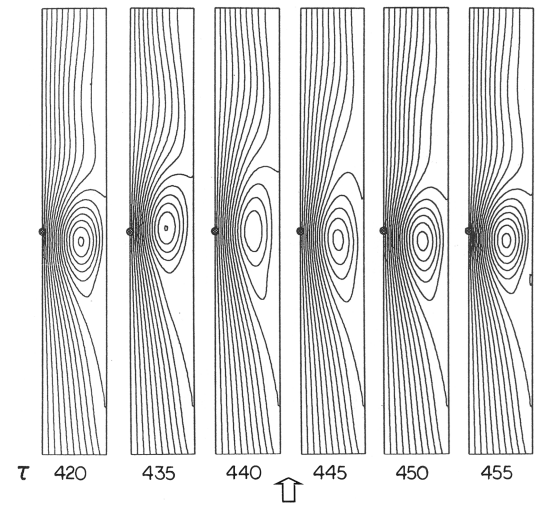

Fig. 7 Variation of flowfield with time for aiding mixed convection flow at $Re = 1200$ and $Gr = 10^5$ ($\Delta\psi = 0.009$).

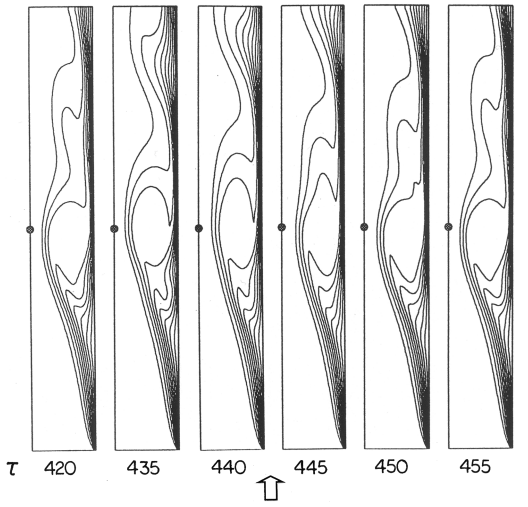

Fig. 8 Variation of temperature field with time for aiding mixed convection flow at $Re = 1200$ and $Gr = 10^5$ ($\Delta\theta = 0.1$).

phenomenon is due to the complicated interaction among three major force fields: electric body force, thermal buoyancy, and flow inertia. The aiding flow is stabilized when the Grashof number is further increased to 10^6. The flow reversal observed earlier (Fig. 5) also occurs in the present case. At $Re = 600$, the variation of flow and temperature fields is very similar to the case of $Re = 1200$, except that the flow and temperature fields for aiding flow at $Gr = 10^6$ do not reach steady state: they exhibit a nonperiodic nature instead.

The heat transfer results for the present study can be examined from the variation of average Nusselt number with time. In addition, the flow transition can also be identified from these curves. Figure 9 displays such information for $Re = 1200$. For flows at $Gr = 10^4$, it is observed that the thermal field oscillates with the same frequency (33.5 units of dimensionless time) as that of the forced convection [5]. It is also observed that the change in Nusselt number is only minimal compared with that for forced convection [5]. As the Grashof number is increased to 10^5, a slight change in the oscillating periodicity is noticed for aiding flow. For opposing flow, on the other hand, the flowfield first exhibits an oscillatory nature, but it gradually dies out and reaches a steady state. It is observed that heat transfer increases in the case of opposing flow compared with that of aiding flow. The enhancement in heat transfer varies from 120 to 140% for $Gr \leq 10^5$. At $Gr = 10^6$, aiding flow experiences a drastic reduction in heat transfer. On the contrary, a steep increase in heat transfer of about 170% is observed for opposing flow. The reason for these dramatic changes can be verified from the contour plots of flow and temperature fields (Figs. 5 and 6). In the case of opposing flows, the recirculating secondary flow is suppressed due to the interaction of primary flow and the buoyancy force, whereas for the aiding flow, the recirculating cell is expanding with an increase in the buoyancy strength. This phenomenon is most prominent at $Gr = 10^6$. The elongated recirculating cell initiates a flow reversal at the channel exit. It is observed that an increase in the thermal buoyancy causes the primary flow to channel through the core region of the flow passage. The temperature contours show an increase in the boundary-layer thickness due to the separation of the primary flow from the wall, which is clearly responsible for the reduction in heat transfer. In the case of opposing flows, with an increase in thermal buoyancy, the EHD-induced secondary flow is effectively suppressed. This helps to keep the thermal boundary layer close to the wall, hence it increases the heat transfer.

The enhancement of heat transfer (compared with that of forced convection) under different intensities of buoyancy force for aiding and opposing flows is summarized in Fig. 10 as a function of the mixed convection parameter Gr/Re^2. The solid symbols represent the steady-state results, whereas the hollow ones are for the steady-periodic results, with their maximum and minimum values indicated as an error bar. For comparison, forced convection results are also included in the figure and are marked on the ordinate (i.e.,

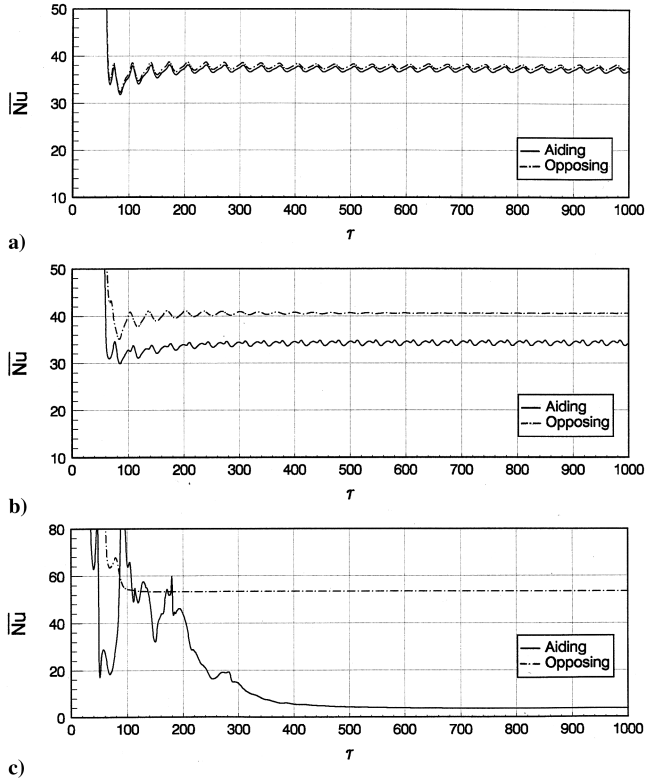

Fig. 9 Variation of average Nusselt number with time for mixed convection flows at $Re = 1200$: a) $Gr = 10^4$, b) $Gr = 10^5$, and c) $Gr = 10^6$.

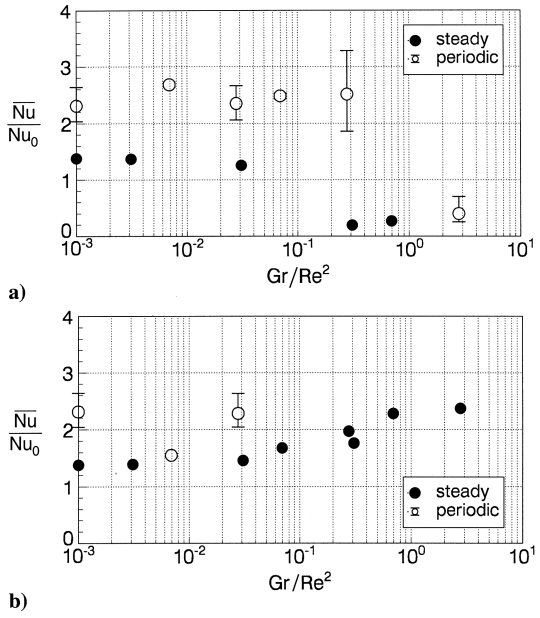

Fig. 10 Heat transfer enhancement by electric field: a) aiding flows and b) opposing flows.

$Gr/Re^2 = 10^{-3}$). As seen from Fig. 10a, for aiding flows, the heat transfer enhancement ratio is less than two for steady-state cases, whereas it is greater than two for steady-periodic cases. When the mixed convection parameter Gr/Re^2 is greater than 0.2, there is a dramatic decrease in the heat transfer rate. As explained earlier, the reduction is due to the entrainment of the ambient air, which effectively blankets the heat transfer surface. For opposing flows, the heat transfer enhancement ratio increases consistently with the mixed convection parameter. When thermal buoyancy is weak (i.e., $Gr/Re^2 < 0.1$), the ratio approaches that of the forced convection asymptote. The ratio is noticeably increased only when thermal buoyancy becomes significant (i.e., $Gr/Re^2 > 0.1$).

Conclusions

Numerical results were presented for mixed convection in a vertical channel under the influence of an electrostatic field. It was observed that the flow and temperature fields resemble those of forced convection when the thermal buoyancy is weak (i.e., $Gr = 10^4$). With an increase in the strength of thermal buoyancy (i.e., $Gr \geq 10^5$), flow and temperature fields may become steady, steady-periodic, or nonperiodic, depending on the direction of the primary flow (i.e., aiding or opposing flows). For aiding flows, heat transfer increases with the thermal buoyancy for flows at $Re = 600$, whereas it decreases for flows at $Re = 1200$ and 1800. The reduction in heat transfer is due to the entrainment of ambient air, which effectively separates the primary flow from the wall. Oscillation in the flow and temperature fields is observed for aiding flows at $Re = 600$ and 1200. The periodicity increases gradually with an increase in the thermal buoyancy. For $Re = 1200$, the flowfield restabilizes at $Gr = 10^6$. For opposing flows, heat transfer is increased for all flow and buoyancy strengths considered. The heat transfer enhancement for opposing flow approaches that of the forced convection asymptote when $Gr/Re^2 < 0.1$ and is increased noticeably only when $Gr/Re^2 > 0.1$. For aiding flows, the trend is not as clear as for opposing flows. However, it is observed that the heat transfer enhancement is greater than two for periodic flows and is less than two for steady flows.

Although the present study examined a fundamental problem in the application of electric field for heat transfer enhancement, the results obtained also have important implications for applications using electrostatic precipitation for gas cleaning or treatment. Because most exhaust gases from industrial applications are usually at an elevated temperature compared with the ambient, it is clear that thermal buoyancy is an important factor in the design of such gas cleaning/treatment systems. If ignored, the buoyancy-induced oscillation and flow entrainment may significantly reduce the particulate collection efficiency of an electrostatic precipitator. To better control the oscillatory flow and flow entrainment, the complicated interaction among electric field, thermal buoyancy, and flow inertia still awaits further investigation.

References

[1] Yamamoto, T., and Velkoff, H. R., "Electrohydrodynamics in an Electrostatic Precipitators," *Journal of Fluid Mechanics*, Vol. 108, July 1981, pp. 1–8.

[2] Lai, F. C., McKinney, P. J., and Davidson, J. H., "Oscillatory Electrohydrodynamic Gas Flows," *Journal of Fluids Engineering*, Vol. 117, Sept. 1995, pp. 491–497.

[3] Takimoto, A., Tada, Y., and Hayashi, Y., "Convective Heat Transfer Enhancement by a Corona Discharge," *Heat Transfer, Japanese Research*, Vol. 20, No. 1, 1991, pp. 18–35.

[4] Lai, F. C., "Effects of Buoyancy on EHD-Enhanced Forced Convection in a Horizontal Channel," *Journal of Thermophysics and Heat Transfer*, Vol. 12, No. 3, 1998, pp. 431–436.

[5] Lai, F. C., and Mathew, J., "Heat Transfer Enhancement by EHD-Induced Oscillatory Flows," *Journal of Heat Transfer*, Vol. 128, No. 9, 2006, pp. 861–869.

[6] Huang, M., and Lai, F. C., "Numerical Study of EHD-Enhanced Forced Convection Using Two-Way Coupling," *Journal of Heat Transfer*, Vol. 125, No. 3, 2003, pp. 760–764.

[7] Yamamoto, T., "Electrohydrodynamic Secondary Flow Interaction in an Electrostatic Precipitator," Ph.D. Dissertation, The Ohio State Univ., Columbus, OH, 1979.

[8] Jaluria, Y., and Torrance, K. E., *Computational Heat Transfer*, Hemisphere, New York, 1986.

[9] Roache, P. J., *Computational Fluid Dynamics*, Hermosa, Albuquerque, NM, 1976.

[10] Peek, F. W., *Dielectric Phenomenon in High Voltage Engineering*, McGraw–Hill, New York, 1966.

[11] Davidson, J. H., and Shaughnessy, E. J., "Turbulence Generation by Electric Body Forces," *Experiments in Fluids*, Vol. 4, 1986, No. 1, pp. 17–26.

[12] Shah, R. K., and London, A. L., *Laminar Flow Forced Convection in Ducts, Supplement 1*, Advances in Heat Transfer, Academic Press, New York, 1978.